Electromechanical Energy Conversion Systems (EECS)
Niroo Research Institute
Vol. 2, No. 1, Winter 2023, 52-69
DOI: 10.30503/eecs.2023.380361.1033
Review Article

Advances in Developing Permanent Magnets with Less or No Rare-Earth Elements

Banafsheh Mirtaheri[1*], Hamed Tahanian[2]

Abstract

Permanent Magnets (PMs) are employed in many modern devices, thanks to their unique properties. Electrical machines, i.e., motors and generators, are a major application of PMs, which produce the required magnetic field. When there are severe constraints on the weight and dimensions of the device (e.g. in hybrid electric vehicles or wind turbines), using high-energy PMs would be of crucial importance. Currently, PMs which contain Rare-Earth Elements (REEs), e.g. Sm-Co and Nd-Fe-B, are the most commonly used and the most powerful practical PMs. However, the monopolized supply of the raw materials required for the production of these PMs as well as the recent rise in their global price, have encouraged researchers to investigate some methods for reducing the consumption of REEs or substituting other PMs for those with REEs. This paper studies the state of the art advances in developing PMs with less or no REEs and the corresponding achievements.

Keywords: Permanent magnets, Rare-earth elements, Electrical machines.

Received Date: *09 January 2023;* ***Revised Date:*** *01 February 2023;* ***Accepted Date:*** *06 February 2023.*

1. INTRODUCTION

Permanent Magnets (PMs) are hard magnetic materials utilized in a broad range of applications such as magnetic storage devices [1], magnetic sensors [2], loudspeakers and microphones [3], Magnetic Resonance Imaging (MRI) devices [4] and industrial cranes [5]. Another application of PMs is in electromechanical energy conversion devices including wind turbine generators [6,7], electric motors applied in Electric Vehicles (EV) and Hybrid Electric Vehicles (HEV) [8], fluid pumps [9], compressors [10], and so on. The optimal performance of the PM devices is proportionally related to the high energy product, high operating temperature, as well as mechanical and chemical stability of PMs. Furthermore, low price, easy to produce, light weight, and non-toxicity of PMs should also be considered when a PM is selected in a particular application [11, 12]. Early PMs were developed from lodestone containing magnetite mineral (Fe_3O_4). Afterwards high-carbon steel, hardened by the rapid cooling of the melt (quenching) was used as a PM [11]. By 1885, a steel containing ~5% tungsten was used as PM, and chromium steel was substitute for it during World War I. However, none of them had coercivity of more than 8 kA/m (100 O_e) [13]. In 1917, it was shown that steel with 30%-40% cobalt along with tungsten and Chromium has a coercivity of 230 O_e with a maximum energy-product of 8 kJ/m^3 (1 $MG.O_e$) [13]. During the 1930s, Alnico PMs were used in place of steel PMs [14]. Despite being brittle, Alnico PMs were of high remanence and relatively high Curie temperature (e.g. 900 ^{0}C for grade 5) which were the main advantages of Alnico over the previously developed PMs [13]. In addition, its maximum energy-product was much higher than that of its previously developed counterparts (e.g. 73.6 kJ/m^3 (9.2 $MG.O_e$) for grade 9) [5]. The most promising PMs after Alnico were ceramic ferrite magnets especially strontium and barium ferrites which were developed in 1950s [14]. In fact, minimum price of ferrites in comparison to other PMs, made them as widely used magnets with approximately 88% of the total weight of the produced PMs in the globe [15], [16]. The maximum energy-product of wet pressed and sintered barium hexaferrite is 30 kJ/m^3 (3.77 MG.Oe), and it has a lower Curie temperature compared with Alnico [17-19]. The invention of rare-earth (RE) PMs in 1960s attracted the global attention towards manufacturing of high-performance electrical machines [11]. In fact, thanks to high energy-product in RE PMs, smaller magnets with high efficiency and high torque density

[1] Department of Materials Science and Engineering, Iran University of Science and Technology (IUST)
[2] R&D Department, Mapna Generator Engineering and Manufacturing Company (PARS)
*Corresponding author email: banafsheh.mt@gmail.com

can be used in electrical machines (Fig. 1) [20]. There are three principal types of RE PMs. Each of them has a much higher maximum energy-product (BH_{max}) compared to non-rare-earth (non-RE) PMs. They are $SmCo_5$, Sm_2Co_{17}, and $Nd_2Fe_{14}B$ (or concisely Nd-Fe-B) [13].

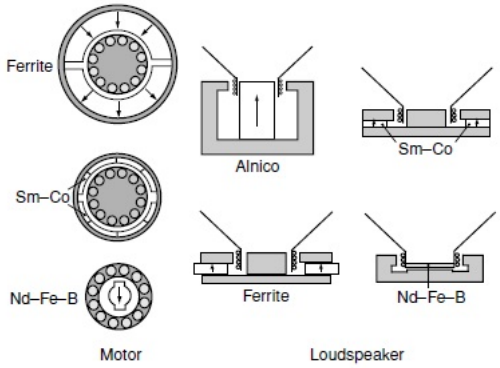

Fig. 1: The effect of the PM type on the design of DC motors and loudspeakers [20]

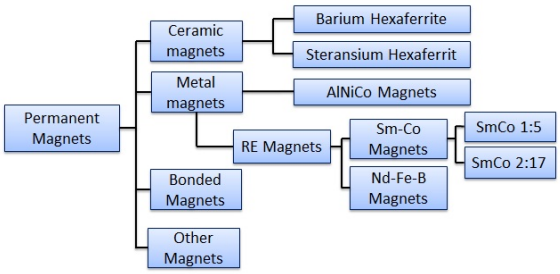

Fig. 2: The classification of PMs

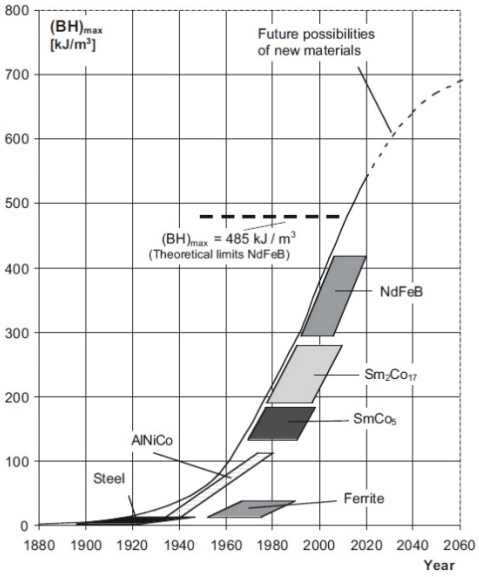

Fig. 3: The development trend of the maximum energy of PMs with time [12]

The values of BH_{max} for $SmCo_5$ and Sm_2Co_{17} are about 18 MGOe (143.2 KJ/m^3) and 22-32 MGOe (175-255 KJ/m^3), respectively (the exact values depend on the composition). Furthermore, their Curie temperatures are 700 and 750 ℃, correspondingly. Currently, Nd-Fe-B magnets are the most powerful PMs, which possess the maximum energy of 56 MG.Oe (445.7 KJ/m^3) and Curie temperature of about 360 ℃ [11]. Classification of PMs and development trend of their maximum energy-product are shown in Fig. 2 and Fig. 3, respectively. Furthermore, Second quadrant of B-H Curves of common PMs are compared in Fig. 4. In 2014, about 67% of all Nd-Fe-B PMs have been consumed for construction of electric motors. The amount of Nd-Fe-B PMs used in some electric motors and generators in 2015 are tabulated in Table 1.

The rare-earth elements (REEs) which are used for the production of RE PMs are in the category of strategic materials. According to the report of the United States Geological Survey (USGS), most of the REEs resources are located in China [22]. This country is also the biggest producer of RE PMs. In 2009, China put some restrictions on the production and exports of REEs [11]. As a result, the price of Nd was increased and reached to its maximum value in the second half of 2011 (see Fig. 5). This dramatically reduced the global production of Nd-Fe-B PMs in the second half of 2011 and early 2012 (see Fig. 6). However, following the reduction of the price of RE elements, the production of these PMs was increased again [16]. The price falling was continued with more intensity in 2015, which has been reported to be the consequence of illegal production of these elements in China. In October 2015, China exported 26800 tons of REEs, which shows a 20% increase compared to the same period in 2014 [22]. According to Table 2, it is observed that the production of REEs has been raised in some countries in 2015 comparing to 2012. However, the price fluctuations implies sort of inconstancy in the market of REEs and PMs containing these elements.

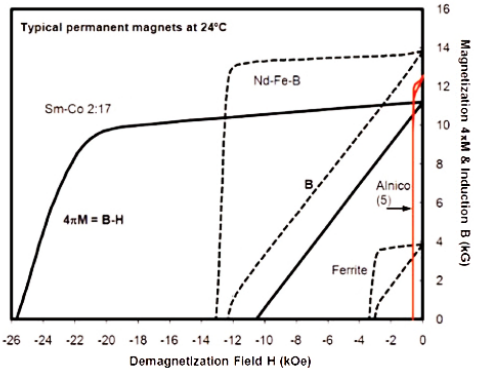

Fig. 4: Comparison of second –quadrant B-H curves for common PMs [21]

In 2018, prices stabilized at 70 USD/kg for Nd and 280 USD/kg for Dy. In 2019 cobalt price was 70 USD/kg, but remains volatile and has fluctuated between 20 and 110 USD/kg over the past 10 years [23]. Fig. 7 shows the amount of supplied REEs as well as the required amount for the production of Nd-Fe-B PMs until 2016. It is clear that after 2006, there has been always a gap between the supply and the demand.

The increased and fluctuating prices of REEs, also regarding their supply monopoly, have encouraged the researchers to seek solutions for reducing the demand for these elements. Among them, the recycling of RE PMs has gained attention recently [24]-[26], which disused PMs are converted to new PMs by direct recycling. In the indirect approach, the REEs of the disused PMs are first extracted by chemical methods and then are used for the production of new PMs [24], [26]. Unfortunately, the recycling process is costly and time consuming, in addition to the fact that the recycling rate may not be very high [25], [26]. In this regard, currently the best solution for the problem is reducing the REEs required for PMs or finding appropriate alternatives for RE PMs. Many studies have been conducted in recent years to find these alternatives. The published report by United States Department of Energy (DOE) in 2011 is explanatory of its investments for finding these substitutes [27]. It should be noted, however, that removing the REEs from PMs implies the deterioration of their excellent magnetic properties. Therefore, it is necessary to adopt special techniques in order to improve the properties of substituted PMs. These techniques are broadly divided into two categories:

- Improving the nano/micro structure of nanocomposite PMs (including exchange bias and exchange spring PMs)
- Improving the crystalline structure to increase the anisotropy (including the $F_{16}N_2$ PMs, magnets with $L1_0$ structure, etc.)
- There is no comprehensive study on different methods to reduce REEs consumption or production of new non-RE PMs. These are addressed in this paper in order to identify the compounds with highest potential for competition with RE PMs.

The improvement of maximum energy-product for Sm-Co and Nd-Fe-B PMs is one of the approaches for reducing the consumption of REEs. Hence, methods of improving this quantity are first described. Then, new PM generations with less or no REEs are introduced and the relevant works are reviewed. These PMs include exchange bias and exchange spring magnets, nitrogen martensite ($F_{16}N_2$), compounds with $L1_0$ structure ($L1_0$ Fe-Pt, $L1_0$ FePd, $L1_0$ CoPt, $L1_0$ FeNi, $L1_0$ MnAl), MnBi and MnGa compounds, carbide-cobalt nano-blades, serum-based compounds, Hf-Co and Zr-Co magnets, and Sm-Fe-N magnets.

TABLE 1: THE AMOUNT OF ND-FE-B PMS USAGE IN 2015 [16].

Application	Consumption in 2015 (Tons)
electric and hybrid vehicles	7000
Wind generators	8500
Electric bicycles (mainly in Asian countries)	6000

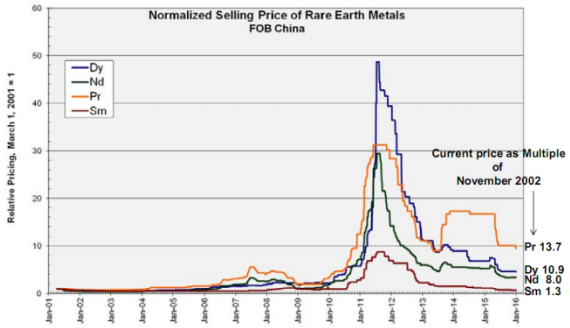

Fig. 5: Variations in the price of some REEs from 2001 to 2016 [16]

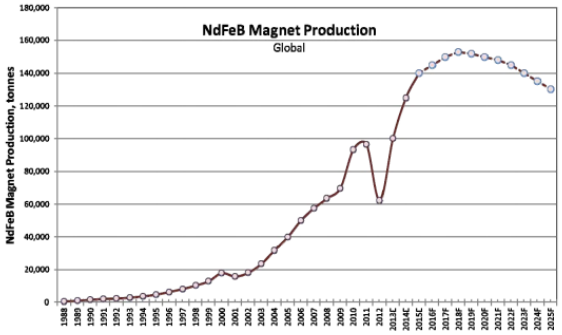

Fig. 6: The mount of Nd-Fe-B PM production in different years [16]

TABLE 2: THE AMOUNT OF PRODUCED ND-FE-B PMS IN DIFFERENT PLACES FOR 2012 AND 2015 [16]

Country/Region	Production in 2012 (tons×1000)	Production in 2015 (tons×1000)
China	50	65
Europe	1	1
Japan	10	8
The USA	0	2
Other countries	2	2
Total	63	78

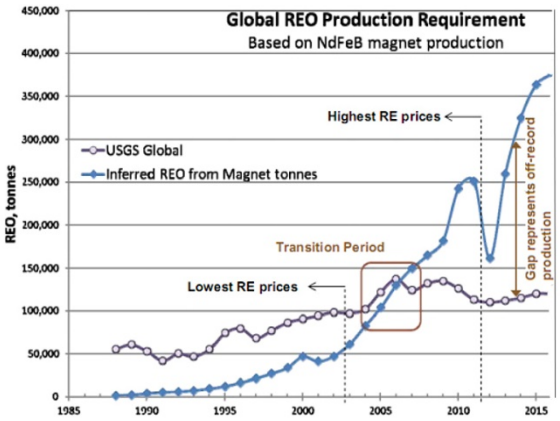

Fig. 7: The mount of supplied REEs versus the demand of these elements for the production of Nd-Fe-B PMs until 2016 [16].

2. EFFECTIVE FACTORS ON THE MAXIMUM ENERGY PRODUCT (BH)MAX

Fig. 8 shows the demagnetization curve of a PM and its energy product as a function of flux density. Generally, effective factors on remanence B_r and coercivity H_c could also affect the $(BH)_{max}$. The following technique could be employed in order to reduce the amount of REEs consumption in RE-PMs and improving their performance:

- Improving the magnetocrystalline anisotropy [28], [29]
- Reducing the size of particles [30]
- Domain wall pinning [13], [30], [31]

These techniques are usual for new generation of PMs.

2.1. Magnetocrystalline anisotropy

The magnetocrystalline anisotropy is an intrinsic property, based on which the magnetization vectors inside a magnetic material tend to align in preferential directions. These are referred as the easy directions of magnetization [14]. Materials with single-axis anisotropy have only one easy direction of magnetization. Bringing the magnetization vectors out of the easy direction requires high energy. Therefore, the PMs, which their particles are arranged and magnetized in the easy direction, possess high B_r [32].

Fig. 9 illustrates the different behavior of materials with axial anisotropy in two cases: 1) when the material is magnetized in the easy direction and 2) when the magnetization and easy direction build an angle. It is obvious that the first case results in a higher $(BH)_{max}$ [32].

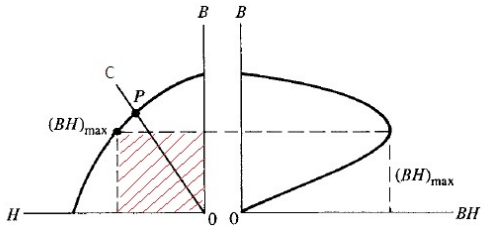

Fig. 8: the demagnetization and (BH)-B curves for a typical PM [13].

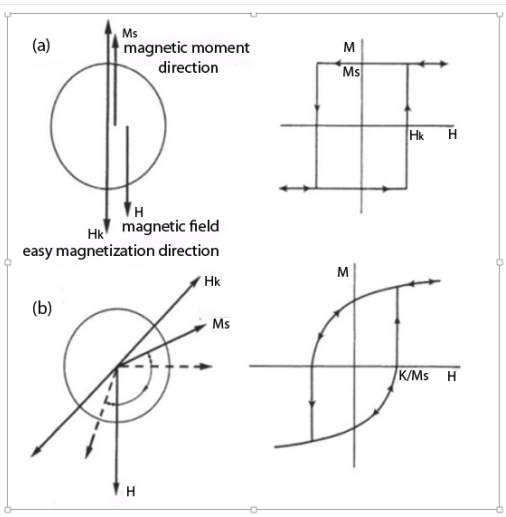

Fig. 9: The behavior of a single-domain material with single-axis anisotropy in two different conditions (a) the material is magnetized in the easy direction (b) the magnetization vector and easy direction build an angle [14], [32].

2.2. Size of Particles

The variation of coercivity with the size of constituent particles of a PM is plotted in Fig. 10. It is obvious that by reducing the size of particle, the coercivity first increased and after a maximum value, it falls. This maximum value is different for materials with various magnetocrystalline anisotropies. This critical size, which is measured in nm, is called the critical single domain size. It implies that the smaller particles only contain one magnetic domain. Since the magnetization vectors in the wall of magnetic domains are not exactly parallel and they show gradual changing direction, their rotation due to the application of an external field requires less energy compared to magnetization vectors inside domains. In fact, when an external field is applied, the direction of magnetic moments inside domains should be changed suddenly, which requires more energy. Therefore, it is expected that the coercive field (H_c) is increased by removing these walls [33], [34]. The reduction of coercive field for very small sized particles is due to the reduction of anisotropy energy. This energy, which lines up the magnetization vectors in the easy direction, decreases

with the reduction of particle volume and the thermal energy dominates it. Accordingly, the magnetization vectors moves from one easy direction to the other [33]. Therefore, in order to achieving the maximum Hc, the size of particles should only be reduced to the critical single domain size, if possible.

2.3. Domain wall pinning

When the field in the second quadrant of M-H curve is reversed, new magnetic domains start to form in the applied field direction. The domain wall may encounter some barriers while moving, which could result the blocked wall (Fig. 11). These factors could be intrinsic (e.g. dislocations in crystalline structure) or external (e.g. secondary phases and impurities). The wall should have enough energy to pass these barriers. In this regard more energy should be supplied to the system, which increases the H_c [20], [35]. In 2022, Zhongwu Liu et al. [36] proposed an annealed Al-Cr coating to simultaneously enhance the coercivity by grain boundary diffusion process and improve the anticorrosion properties by surface protection. Al62.5Cr37.5 coating was deposited on the Nd-Fe-B substrate followed by an annealing treatment at 550 °C. Al element mainly segregates at the grain boundary region. This results in *H*cj and $(BH)_{max}$ increments of 89 kA/m and 3.4 kJ/m3, respectively.

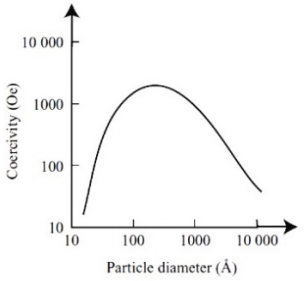

Fig. 10: Coercivity as a function of the size of small particles [33].

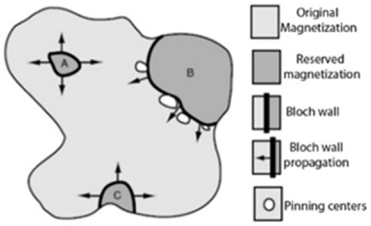

Fig. 11: Reversing the magnetization vectors in the second quadrant. The B domain is faced with the domain wall blocking factors [20].

3. IMPROVING THE PROPERTIES OF RE-BASED PMS FOR REDUCING THEIR CONSUMPTION

Some research have been conducted on improving the magnetic properties of Sm PMs by changing in their synthesis method, as well as modifying their chemical composition. Table 3 summarizes some of the obtained results.

In the case of Nd-Fe-B PMs, employing the fast cooling (melt spinning), which is known as magnequench, has improved the properties. In this method, the Nd-Fe-B alloy is melted and by the pressure of argon gas (Ar) is spread on the surface of a water cooled wheal through a tiny slit. This cools the molten material very fast (rate of 10^4-10^7 K/s) and hence, thin strips of the alloy are formed [11], [14]. Each grain in the flake like particles is of single-domain type, which increases the coercively of the PM [30]. Finally, the obtained sheets are shaped as bulk pieces [14].

The other manufacturing method of single-domain particles in order to increase the $(BH)_{max}$ of the PM is Hydrogenation-Disproportionation Desorption-Recombination (HDDR) By using this process it is possible to achieve a fine microstructure such as the melt spinning method. For this purpose, it is necessary to heat up the PM powder at the hydrogen atmosphere to 750 °C. This converts the $Nd_2Fe_{14}B$ composition inside the grains into a fine mixture of $NdH_{2.2}$, Fe, and Fe_2B. In the next step, the material is evacuated and after the hydrogen removal, the aforementioned compositions are reconverted to $Nd_2Fe_{14}B$. Accordingly, the size of each particle would be about 0.3 μm, which is very close to the single domain critical size (0.26 μm [32]) [30]. This process is schematically shown in Fig. 12.

Furthermore, several atomic substitutes have been proposed for improving the magnetic properties of Nd-Fe-B PMs, which include:

TABLE 3: SOME OF THE MODIFICATIONS IN THE MIXTURE AND THE SYNTHESIS METHOD OF SM PMS FOR IMPROVING MAGNETIC PROPERTIES

Modification	Result	Reference
Inserting nitrogen atom in the interstitial sites of Sm_2Co_{17} structure	Increased magnetization, anisotropy, and Curie temperature	[13]
Adding Fe	Increased M_s	[30]
Adding Zr	Improved H_{ci}	[30]
Adding nitrogen and creating the $Sm_2Fe_{17}N_3$ composition	Increased $(BH)_{max}$ up to 59 MGOe (470 KJ/m^3) in theory and 20 MGOe (470 KJ/m^3) in practice	[11]
Synthesis of Sm_2Co_{17} by ball milling the $SmCo_5$ with high energy	Increased H_c up to 8.3 KOe	[37]

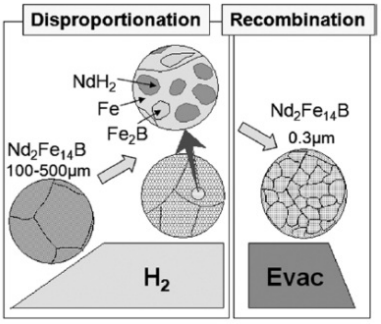

Fig. 12: The schematic of HDDR process [38].

- Substituting other REEs for Nd,
- Substituting other metals or non-metals for Fe,
- Substituting other non-metal elements for B.

In this regard, various types of these PMs have been produced, which were discussed with details in [39].

4. New Generation of PMs

4.1. Exchange bias and exchange spring PMs

These PMs are constituted from at least two magnetic phases with desirable properties, which have been mixed with other in nanometric scale. In this manner, it is possible to use their advantages at the same time [5]. This is due to existence of quantum mechanical exchange force (exchange interaction) between the two magnetic nanomaterials. Exchange forces are the source of other anisotropy in materials, which are called the exchange anisotropy. This factor, besides the other sources of anisotropy and coercivity improving factors, results in higher H_C and hence higher $(BH)_{max}$. These nanocomposite PMs are divided into exchange bias and exchange spring categories [11], which are described in the following.

4.1.1. Exchange bias PMs

In these PMs, which are also known as nanocomposite PMs, a ferromagnetic (FM) phase and an antiferromagnetic (AFM) phase with high magnetic anisotropy constant (high K_1) are mixed together in nanometric scale. The first spin layer of AFM is parallel to FM spines and the next spin layers are arranged parallel to each other, but with opposite directions [40]. When the magnetic field is reversed, the FM spins start to turn. However, if AFM possess considerable anisotropy (high K_{AFM}), its spines stay at their place. Therefore, due to the exchange coupling phenomenon, an additional torque is applied to the FM spines, which tend to preserve their direction (Fig. 13(b)). Accordingly, the required field for reversing the FM magnetization is higher compared to the non-coupled case, which implies a high H_c in negative direction (Fig. 13(c)). When the field is reversed again and becomes positive, the rotation of FM spines would be easier than the non-coupled case, because of the interaction with AFM spines (Fig. 13(d)). This reduces the coercivity in positive direction. The final result is a shift in the hysteresis loop to the left side of vertical axis. Therefore, the $(BH)_{max}$ is increased for the second quadrant [38]. The shifted loop has been compared with the original loop of the ferromagnetic material in Fig. 14 (right side).

For the improvement of exchange bias, it is desired that the nanometric particles have the largest possible contact surface. In this regard, particle with the high surface to volume ratio are more appropriate. The best result is obtained when the diameter of ferromagnetic material is twice the antiferromagnetic material domain wall width. Much thicker ferromagnetic material makes the exchange coupling phenomenon to be not effective [11].

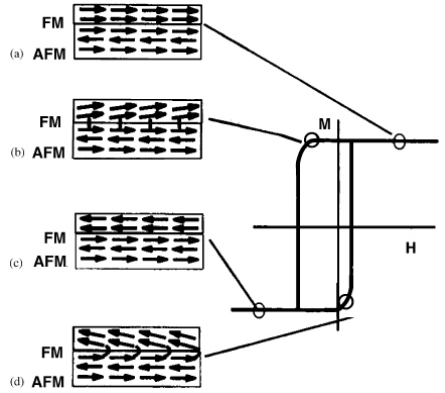

Fig. 13: The arrangement of FM/AFM couple spines in exchange bias PMs with the field variations [40]

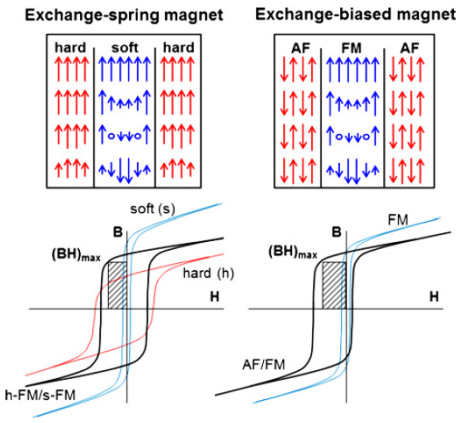

Fig. 14: the change in hysteresis loops of exchange bias and exchange spring PMs [11]

Mn-based alloys are suitable choices for producing exchange bias PMs. Recent efforts have been focused on the synthesis of nanocomposits, which their ferromagnetic phase is based on Fe and their antiferromagnetic phase are CuMn, AgMn, CoMn, and IrMn. Non-equilibrium methods, such as melt spinning and mechanical milling, are required for creation of semi stable phases and increasing the solid dissolution of Mn in the alloy.

Another example of these PMs is the nanocomposite obtained by fast cooling of Fe-Co-Mnalloy, where a ferromagnetic phase of α-FeCo and an antiferromagnetic phase enriched with γ-Mn are produced. The H_c of this system is raised to 350 Oe, which is considerably higher than the H_c of α-FeCo phase. It is expected that lengthening the ferromagnetic sediments through the application of external field during heat treatment process would result to an increased shape anisotropy and improved $(BH)_{max}$ [5][11].

4.1.2. Exchange spring PMs

In these PMs, one of the nanophases is a soft ferromagnetic material and the other is a hard ferromagnetic material. This results to a wide hysteresis loop (the left side of Fig. (14)). At the beginning, the magnetic moments of both phases are in the same direction. When the magnetic field is reversed, the spines of soft phase tend to rotate, as shown in Fig. 15. However, their coupling with hard phase spines opposes this rotation. Therefore, an additional energy is required for rotating them, which implies a raised coercive force. When the reverse field is high enough, the moments of the hard phase also arrange in the reverse direction. When the applied field becomes positive, a similar behavior is observed. This makes the hysteresis loop to be wider [40].

The ideal structure for exchange spring composites is that a large amount of soft magnetic nanoparticles are distributed in a matrix of the hard magnetic material. The geometry of soft magnetic phase affects the final properties. If the soft phase has a cylindrical shape and is distributed in a substrate of the hard magnetic material, the maximum value for $(BH)_{max}$ is obtained. When the soft phase has a spherical shape, this quantity is minimized [41].

The magnetic energy of these PMs is calculated by (1). Because of factors such as impurities and homogenity of phases and their crystalline orientation, actual values are a bit different with the theoretical ones.

$$(BH)_{max} = \frac{1}{4}\mu_0 M_s^2 \left[1 - \frac{1}{2}\frac{\mu_0 (M_s - M_h) M_s}{K_h}\right], \qquad (1)$$

Where, M_h and M_s are the magnetizations of soft and hard phases, respectively. Also, K_h is the anisotropy constant of the hard magnetic phase.

Another microstructure used for producing soft/hard magnetic composites is the core-shell structure, which is shown in Fig. 16. In this microstructure, a nanoparticle of one of the soft or hard phases is placed at the center and the other phase covers it [42]. The exchange spring phenomenon could also be exploited for reducing the amount REEs consumption in PMs with high $(BH)_{max}$. By combining $Nd_2Fe_{14}B$ with soft magnetic phase α-Fe, it is possible to simultaneously benefit from the high magnetization of iron phase and the high magnetocrystalline anisotropy of $Nd_2Fe_{14}B$ phase [11]. Ideally, these PMs with high degree of crystal orientation would have triple the magnetic energy compared to the commercial Nd-Fe-B PMs and, at the same time, more resistance to corrosion and lower price. For producing such PMs, iron particles smaller than 10 nm should be dispersed inside a matrix of hard magnetic phase containing REEs. Manufacturing anisotropic PMs from these materials is still a challenge [5]. Many researches have been conducted on producing exchange spring nanocomposite PMs with high $(BH)_{max}$ in order to reduce the amount of REEs. Table 4 summarizes the important result of these studies.

The exchange spring made of L10 type MnAl(C)/α-FeCo could also be a good alternative for RE PMs. This PM is expected to have a Curie temperature of 277 °C and coercivity of 200-300 kA/m [5][52].

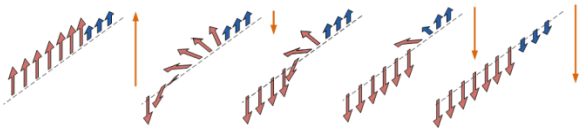

Fig. 15: the change in direction of magnetization vectors of soft magnetic material (red) and hard magnetic material (blue) for exchange spring PM

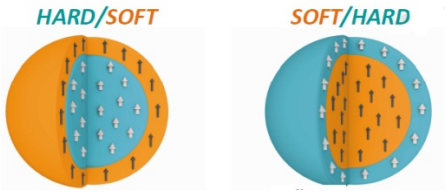

Fig. 16: the core-shell structure for soft/hard magnetic composite [42].

TABLE 4: EXCHANGE SPRING PMS AND THEIR MAGNETIC PROPERTIES

Nanocomposite	$(BH)_{max}$ (MGOe, KJ/m^3)	Improvement comparing to the base composition (%)	Reference
Anisotropic Multi-layer films of $[Nd_2Fe_{14}B/Ta/Fe_{67}Co_{33}/Ta]_n$	~63 MGOe ~500 kJ/m^3	-	[43]
Multi-layer film of $L1_0$ FePt/$Fe_{45}Co_{55}$	50 MGOe (actual) 85.1 MGOe (theoritical)	~233% ($(BH)_{max}$ FeP ~15 MGOe)	[44]
Fe/SmCo5	50.25 MGOe 400 Kj/m^3	74% ($(BH)_{max}$ SmCo5=230 Kj/m^3)	[45]
α-Fe/$Sm_2(Fe,Si)_{17}C_x$ (synthesized at pressure of 3 GPa)	25 MGOe 199 Kj/m^3	-	[46]
Isotropic FePt/Fe_3Pt	20 MGOe 160 Kj/m^3	53% ($(BH)_{max}$ FePt=13 MGOe)	[47], [48]
FePt/Fe	20 MGOe 160 Kj/m^3	-	[49]
Zr_2Co_{11}/FeCo	19.5 MGOe 156 KJ/m^3	17.5% ($(BH)_{max}$ Zr_2Co_{11}=16.6 MGOe)	[50]
$SrFe_{12}O_{19}/Fe_3O_4$	0.226 MGOe 1.8 Kj/m^3	37% ($(BH)_{max}$ $SrFe_{12}O_{19}$=0.165 MGOe)	[51]
$L1_0$ type MnAl(C)/α-FeCo			[52]
$Co_{0.6}Zn_{0.4}Fe_2O_4/SrFe_{10.5}O_{16.75}$	1253 Oe emu/g	53% ($(BH)_{max}$ $SrFe_{10.5}O_{16.75}$=817 Oe emu/g)	[53]
$CoFe_2O_4$/FeCo	3.7 MGOe 29.4 kj/m^3	50% ($(BH)_{max}$ $CoFe_2O_4$=19.5 Kj/m^3)	[54]

4.2. Ordered Nitrogen Martensite PM (α‘-Fe16N2)

This material, which was introduced in 1972, has a considerably high magnetic moment (3 μ_B/atom). α‘-$Fe_{16}N_2$ is usually obtained through the fast cooling of nitrogen austenite phase (γ-FeN) followed by the heat treatment at low temperature (127-202 °C). In this composition, nitrogen atoms are inserted in the iron structure. This phase is one of the best substitutes for RE PMs. However, lack of α‘-$Fe_{16}N_2$ stable phase has been the main challenge during the previous years, since this material is semi stable and decomposes into α-Fe and Fe_4N at 200-300 °C. This compound gained attention in 2011 after the publication a report on successful and repeatable synthesis of this phase with the purity of 91%. For this synthesized PM, M_s is 221 emu/g at room temperature. Obtaining the pure phase of α‘-$Fe_{16}N_2$ was impossible until 2012, due to low dissolution of nitrogen atom in austenite structure [11]. In 2013, the pure single-phase of this compound was made, with the reproduction capability at gram scale, through the iron oxide reduction method and then, its nitridation at a low humidity atmosphere with low oxygen. High saturation magnetization (M_s=234 emu/g at temperature of 5 K) and considerable magnetocrystalline anisotropy constant (K_1=9.6×10^6 erg/cm^3) have made it appropriate for replacing RE PMs [28]. Other studies on its synthesis have been also conducted [55], [56], [57], [58].

Calculations and experiments have shown that adding manganese impurity could increase the thermal stability of α‘-$Fe_{16}N_2$ phase. It was reported in a patent published in 2011 that $(BH)_{max}$ of this phase could reach to 135 MGOe (1074.5 KJ/m^3), which is twice the corresponding value of Nd-Fe-B PM [60]. However, the actual $(BH)_{max}$ of this compound is lower. In 2016, the bulk piece of α‘-$Fe_{16}N_2$ prepared by the strained-wire method showed a $(BH)_{max}$ of 9

MGOe (71.64 KJ/m^3) [56] and this quantity for $Fe_{16}N_2$ foil made by nitrogen ion-implantation technique was 20 MGOe (160 KJ/m^3) [55]. The α‧ - $Fe_{16}N_2$ compound which is synthesized by reduction and nitridation of γ-Fe_2O_3 has also the semi hard magnetic property with $(BH)_{max}$ of 3.5 MGOe (28 KJ/m^3) and 361 °C Curie temperature [57].

4.3. Compounds with L10 Structure

The $L1_0$ structure is a crystalline structure which is formed in many equiatomic compounds. In this structure, there are variable layers of the two constituent elements of the composition, which are arranged parallel to the C-axis of the tetragonal structure. Therefor a natural superlattice is created (right side of Fig. 17). In fact, the ordered $L1_0$ structure is obtained from the atomic arrangement of a disordered face centered cubic (fcc), which is called A1 (left side of Fig. 17). Fe-Pt, Fe-Pd, Co-Pt, Fe-Ni, and MnAl have such a structure and are good alternatives for RE PM. Although these materials have high magnetization and considerable magnetocrystalline anisotropy, they have not been commercialized yet due to technological problems, such as difficulty in converting the disordered A1 phase to the stable ordered $L1_0$ phase. If the chemical order could be achieved in this structures, they would be advanced PMs with no REEs and high thermal stability [11]. The various members of this family are discussed in the following.

4.3.1. L10 CoPt, L10 FePd, L10 Fe-Pt PMs

This PMs have high magnetization and considerable magnetocrystalline anisotropy. The $(BH)_{max}$ of the $Fe_{58}Pt_{42}$ nanoparticles is 14.7 MGOe (117 KJ/m^3) [11]. $L1_0$ FePt with high uniaxial anisotropy (K_u=3×10^7 erg/cm^3) has also been synthesized. It has shown a proper rectangular hysteresis loop [29]. It should be noted that this materials have been studied only in film shape and for magnetic recording applications [11] [29] [61]. The reason is the high price of Pt and Pd, which limits the employment of these PMs in motors and generators [11].

4.3.2. L10 FeNi

The $L1_0$ crystalline structure of iron-nickel compound, which is also called tetrataenite (Fig. 18), was first discovered in 1960. In general, Fe-Ni compounds are known as soft magnetic materials, but the establishment of $L1_0$ structure with tetragonal lattice in this equiatomic system results in considerable increase in the magnetocrystalline anisotropy [11], [62]. The transformation temperature of disordered A1 structure to ordered $L1_0$ structure for FeNi compounds is 320 °C [52]. Since tetrataenite has relatively high magnetocrystalline anisotropy energy (3.2×10^6 ergs/cm^3 [11] to 7×10^6 ergs/cm^3 [63]) and also possess a magnetization equal to $Nd_2Fe_{14}B$ [52], it is expected as an excellent candidate for RE PMs replacement. The maximum calculated theoretical energy for this compound is 42 MGOe [64]. Table 5 compares some of its magnetic properties with $Nd_2Fe_{14}B$. In contrast with Nd-Fe-B magnets, the hard magnetic properties of tetrataenite show very small variations with the temperature [65]. It should be stated that the magnetic properties of this material depend on the stoichiometry, structural order, and its tetragonal lattice parameters (a, b, and c) [63].

An important point about $L1_0$ FeNi is that this structure could not be obtained in usual laboratory conditions, but it requires the super slow cosmic cooling speeds (in range of million years), which is often provided in meteorites. Therefore, this compound is naturally found in stony, stony-iron, and iron meteorites. The dimensions of tetrataenite phase in stone-iron meteorites, which have been cooled lowly is 10μm [11], [52]. 95% of the volume of NWA 6259 meteorite, which is in North West of Africa, is composed of tetrataenite [65].

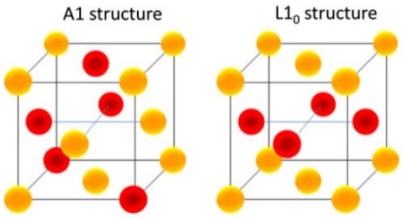

Fig. 17: the schematic of crystalline structure of A1 and $L1_0$ [11].

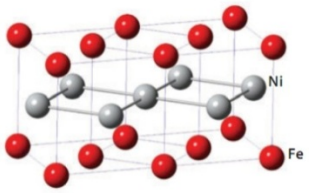

Fig. 18: the crystalline structure of tetrataenite ($L1_0$ FeNi) [52]

TABLE 5: COMPARISON OF SOME MAGNETIC PROPERTIES OF TETRATAENITE ($L1_0$ FENI) WITH $ND_2FE_{14}B$ [63].

compounds	M_s(emu/cm^3)	uniaxial magnetic anisotropy energy (10^{7}erg/cm^3)	Curie temperature (°C)
$L1_0$ FeNi	1270	1.3	>550
$Nd_2FE_{14}B$	1280	4.9	315

Many researches have been done for extracting this compound from this meteorite [64], [65], [66] and its theoretical $(BH)_{max}$ has been obtained about 40 MGOe [65]. Enrichment of the Fe-Ni phase with iron results in an increase in its uniaxial magnetocrystalline anisotropy (Ku) [63]. In this regard, iron enriched tetrataenite ($Fe_{55}Ni_{44}$), which is extracted from NWA 6259 meteorite, possess the theoretical magnetic energy of 42 MGOe (355 KJ/m^3) [64].
It should be noted that tetrataenite has been synthesized in special laboratory conditions by using some techniques, including: magnetron sputtering [67], neutron bombardment of FeNi compound (K_u=3.2×10^5 J/m^3=3.2×10^6 ergs/cm^3) [68], and alternate monatomic layer (ML) deposition of Ni and Fe (K_u=6.3×10^6 ergs/cm^3 [69] and K_u =1×10^6 ergs/cm^3 [70]). However, these techniques are not so much adequate for producing practical PMs. The enrichment of this phase of iron in these techniques is also effective in improving the properties, so that M_s and K_u values for $Fe_{60}N_{40}$ have been reported to be 1470 emu/cm^3 and 9.3×10^6 erg/cm^3, respectively

4.3.3. L10-MnAl

The manganese-aluminum compound with $L1_0$ crystalline structure (Fig. 19) was discovered in 1950s by Kono as well as Koch et al. this compound and MnAlC, which contain some interstitial carbon, have high H_c and $(BH)_{max}$ (theoretical value of 12 MGOe [52]), high corrosion resistance, and low price. Accordingly, they are suitable to be used as advanced PMs. The L10 τ-AlMn tetragonal phase is the only ferromagnetic phase of this compound [11]. This phase possesses a relatively high magnetocrystalline anisotropy constant (K_1=1.7×10^6 J/m^3 [5]), but its M_s is 40% of the corresponding value for $Nd_2Fe_{14}B$ [52]. The ferromagnetic nature of this material originates from Mn Atoms [11].
The ordered $L1_0$ MnAl compound is obtained through the heat treatment of the high-temperature ε-MnAl at 427-627 ℃ [5]. The cooling rate should be higher than 10 °C/s in order to achieve the hexagonal phase [72]. Nonequilibrium synthesis techniques could provide such conditions.
Adding carbon in interstitial sites of MnAl Crystal structure reduces the Curie temperature and magnetocrystalline anisotropy, but it raises the saturation magnetization (M_s) and increases stability of tetragonal $L1_0$ structure [11]. For instance, adding 0.5 wt. % of carbon atom to τ-MnAl decreases the anisotropy field from 55 kOe to 39 kOe and the Curie temperature from 380 °C to 285 °C [52].
This material has been synthesized by the following methods:

- melt spinning: H_c in the range of 1500-2000 Oe and $(BH)_{max}$ approximately 4-7 MGOe (37-56 kJ/m^3) [11],
- mechanical milling: results in the reduction of MnAl(C) grains size and raises H_c. Using this method, H_c has increased from 1000 Oe to 4800 Oe (79.58 kA/m to 382 kA/m) [73],
- gas atomization process [74],
- fast cooling process [74],
- Spark Plasma Sintering (SPS) [75],
- Mechanical alloying by planetary high-energy ball mill [76].

Although MnAl PMs have acceptable performance and low price, but their properties should be improved in order to compete with existing PMs. One approach is to create exchange spring PMs by their composition with α-Fe or FeCo soft magnetic materials. In this way it is possible to produce PMs with $(BH)_{max}$ in the range of 10-15 MGOe (80-120 kJ/m^3), which could be alternatives of low grade Nd-Fe-B magnet (isotropic one). It is expected that in optimal conditions, the Curie temperature of this exchange spring PM is about 300 °C and its magnetic properties are satisfactorily preserved up to 127°C [11].
In addition to MnAl compounds with L0 crystalline structure, some of the other manganese alloys have also shown proper properties for replacing RE PMs. They are discussed in the following.

4.4. MnBi

The low temperature phase of manganese-bismuth is crystallized in hexagonal structure as shown in Fig. 20. It has a high magnetocrystalline anisotropy field (K_1=1.2×10^6 J/m^3, at room temperature) [52]. The theoretical $(BH)_{max}$ for this material has been mentioned to be more than 17 MGOe (135.3 kJ/m^3) [77], [78]. This value is close to the reported $(BH)_{max}$ in a 1988 patent, where the MnBi magnet has been synthesized by directional solidification technique and with particles of the single domain dimensions, equal to 250 nm [79], [80].

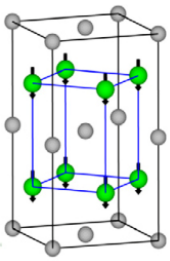

Fig. 19: two unit cells of the $L1_0$ MnAl tetragonal structure [71].

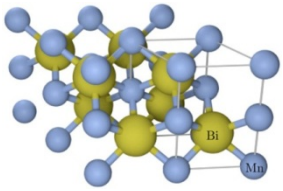

Fig. 20: The crystalline structure of MnBi

An important point about this compound is that its H_c is increased with raising the temperature (K_1 at room temperature and 400 °K is equal to 1.2×10^6 and 2.2×10^6 J/m^3, respectively. Also, $\mu_0 H_c$ is 5 T and 9 T for room temperature and 450 °K) [81], [82]. However, Mn reacts with oxygen when the temperature is high, and formation of MnO weakens the magnetization. Therefore, the temperature rise eventually results in $(BH)_{max}$ reduction [83]. The MnBi phase decomposes at 360 °C, which limits its Curie temperature [71].

The low melting point of Bi on one hand and the high vapor pressure of Mn and Bi on the other hand, have caused some challenges in synthesis and processing of this compound. MnBi could be synthesized by the rapid quenching techniques, but this makes the grain orientation to be isotropic and hence, lowers the $(BH)_{max}$ [52]. The B_r and $(BH)_{max}$ values for MnBi nanostructured powder are 0.25 T and 14 kJ/m^3 (1.76 MGOe), respectively [5].

Spark Plasma Sintering (SPS) is the other synthesis method for this material. The increase of bismuth in the compound results in better formation of the intended phase and improves M_s and M_r, but has a negative effect on H_c ($Mn_{100-x}Bi_x$ (x=40, 45, and 52)) [84]. The nanostructured MnBi has also been synthesized with grain size of 20-30 nm by melt spinning method [80]. Also, its $(BH)_{max}$ is 7.1 MGOe (56.5 kJ/m^3)after combining with epoxy resin and orienting in an applied field [71].

Generally, the $(BH)_{max}$ of MnBi magnet is not high compared to SmCo and NdFeB, and even some other types of PMs. However, thanks to a high magnetocrystalline anisotropy, it is a good candidate for producing exchange spring PMs. It is expected that the MnBi nanocomposite possess a $(BH)_{max}$which is theoretically higher than the corresponding value for NdFeB PM containing Dy [85].

It should be noted that the raw materials cost of MnBi is more than MnAl. In 2014, the cost of these materials was reported to be 15 $/kg and 4 $/kg for MnBi and MnAl, respectively [71].

4.5. MnGa

The other manganese-based compound, which could be employed as a permanent magnet is the manganese-gallium. Although the magnetic properties of this material could not compete with Nd-Fe-B and Sm-Co PMs, it has superior performance compared to some grades of Alnico magnets and some of its parameters are comparable with hexaferrite [86]. If a square hysteresis loop could be attained, the $(BH)_{max}$ of this material would be 25.12 MGOe (200 kJ/m^3) [87]. MnGa is crystallized in three tetragonal crystalline phases: $L1_0$-MnGa (ferromagnetic), $D0_{22}$-Mn_3Ga (ferrimagnetic), and $D0_{22}$-Mn_2Ga [88], [71]. Among them, $L1_0$-MnGa possesses a higher $(BH)_{max}$ and more suitable properties for producing PMs [88], [89]. Theoretically, this structure shows a M_s of 845 emu/cm^3 and a $(BH)_{max}$ of 28 MGOe (222.88 kJ/m^3) [90]. However, the $D0_{22}$ structure, e.g. $D0_{22}$-Mn_3Ga, has a higher H_c due to domain wall pinning mechanism and hence, is a better choice for creating exchange spring PMs [31]. When MnGa compound are synthesized as films, possess higher H_c compared to bulk form [91]. In general, the magnetic properties of MnGa compound strongly depend on the Mn:Ga ratio and the substrate substance on which the film has been formed [31]. Among the various substrate, Si/SiO_2 is more suitable for constituting MnGa with high H_c, since this material grows on it as separate islands [91], [92].

The crystalline structure of $L1_0Mn_xGa$ ($1<x<1.8$) is depicted in Fig. 21. The $(BH)_{max}$ value for $L1_0Mn_{1.5}Ga$ film, which has been synthesized at 300 °C on a gallium-arsenic substrate, is equal to 2.6 MGOe (20.7 kJ/m^3) [86].

The Mn2Ga with $D0_{22}$ (Fig. 22) has a Curie temperature of more than 497 °C, M_s of 0.47 MA/m, and K_1 of 2.35 MJ/m^3. Table 6 compares some properties of this compound with MnAl and MnBi [71].

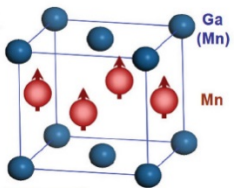

Fig. 21: The crystalline structure of $L1_0Mn_xGa$ ($1<x<1.8$) [86].

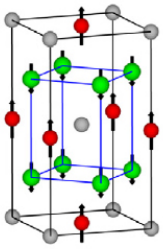
Fig. 22: The crystalline structure of $D0_{22}$ Mn_2Ga (the green and red spheres shows Mn atoms with different magnetic directions) [71].

TABLE 6: COMPARISON OF SOME PROPERTIES OF MNAL, MNBI, AND MN_2GA COMPOSITIONS [71], [88], [31].

	MnAl ($L1_0$)	**MnBi**	**MnGa ($L1_0$)**	**Mn_2Ga ($D0_{22}$)**
Curie temperature ℃	377	360 (phase transformation temperature)	356	phase transformation temperature>497
M_s(MA/m)	0. 60	0.58	0.61	0.47
K_1(MJ/m^3)	1.7	0.9	-	2.35
raw material cost ($/kg)	4	15	-	120

4.6. Other compounds Based on Cobalt

4.6.1. Cobalt Nanorods and Cobalt-carbide Nanoparticles

Polyol processed cobalt nanorods have an almost square hysteresis loop. The $(BH)_{max}$ of this material has been reported to be 20.73 MGOe (165 kJ/m3) and hence, it could be a good substitute for RE PMs [93].

The magnetocrystalline anisotropy of cobalt is increased by adding carbon [94]. The carbide cobalt phases synthesized by polyol reduction chemistry method have a H_c of 4.3 kOe at room temperature and a $(BH)_{max}$ higher than 2.5 MGOe (20 kJ/m^3). These particles are constituted from Co_2C and Co_3C nanophases and their Currie temperature is 273 °C. The high H_c of these compounds roots in the dipolar and magnetocrystalline anisotropies of carbide phases. Their production is at early stages [95], [96].

4.6.2. Hf-Co and Zr-Co Magnets

Recently, some researches have been done on the possibility of replacing magnetic materials containing REEs with the cobalt-enriched transition metal alloys, e.g. $HfCo_7$ and Zr_2Co_{11}, The magnetization of these materials is comparable to Sm-Co. these compounds are crystallized in non-cubic structure with high anisotropy, but their anisotropy is lower than Sm-Co [97]. Instability and the requirement of a high temperature in the range of 1050-1230 °C for $HfCo_7$ production, implies that accurate control of chemical composition and fast cooling process after the alloy formation are necessary to obtain the pure phase. In case of Zr_2Co_{11}, which is formed at 300-1254 °C temperature range, the annealing process at high temperature followed by fast cooling is required to obtain the crystalline structure with considerable anisotropy. It seems that melt spinning and gas-aggregation-type cluster deposition, in which non-equilibrium conditions are established, could be promising techniques for synthesis of $HfCo_7$ and Zr_2Co_{11} nanostructures [98]. Some magnetic properties of $HfCo_7$ and Zr_2Co_{11} compounds are given in Table 7.

The $(BH)_{max}$ of Zr_2Co_{11} is 16.6 MGOe (132 kJ/m^3). It has been observed that by making exchange spring composite PMs using Zr_2Co_{11}/FeCo, the $(BH)_{max}$ is raised to 19.5 MGOe (156 kJ/m^3) [50].

4.7. Cerium-Based PMs

Among the REEs, cerium, lanthanum, and to some degree, praseodymium (pr) are more available than others. In fact, cerium has a portion of 40% of REEs existing in the earth's crust. The concentration of cerium in light-REEs deposits reaches to 50%. In contrast, Dy, which is used for manufacturing Nd-Fe-B PMs, contributes to just 2% of REEs resources and is only found in specific areas. The development of PMs, in which Ce is used instead of Nd and Dy, could be a good advancement in this field [52]. Enormous investments and research collaborations of U.S. Department of Energy (DOE) on cerium-based PMs from 2011 expresses the importance of these materials [27], [99], [100]. However, researches have revealed that replacing Nd in Nd-Fe-B PMs entirely by cerium causes sharp decline of magnetocrystalline anisotropy, Curie temperature reduction, and 15% decrease in the saturation magnetization [99], [101], [102]. $Ce_{12}Fe_{28}B_6$ has a $(BH)_{max}$ of 5.57 MGOe (44.33 kJ/m^3), which shows a 73.56% reduction in comparison with $Nd_{12}Fe_{82}B_6$ produced by the same method. By increasing the cerium to iron ratio in this compound ($Ce_{13.5}Fe_{28}B_6$), the $(BH)_{max}$ value approaches to 6.8 MGOe (54.13 kJ/m^3) and the hysteresis loop is almost square (0.85% squareness) [101], [102].

TABLE 7: SOME MAGNETIC PROPERTIES OF $HFCO_7$ AND ZR_2CO_{11} [5]

material	**B_r(T)**	**$\mu_0 H_c$ (T)**	**$(BH)_{max}$ ($\times 10^3$ J/m^3)**
Zr_2Co_{11} isotropic ribbons	0.6	0.2	42
Zr_2Co_{11} aligned nanoparticles	0.84	0.44	132
$HfCo_7$ isotropic ribbons	0.7	0.2	35
$HfCo_7$ aligned nanoparticles	0.9	0.45	100

Sintering a mixture of $Ce_2Fe_{14}B$ and Nd-Fe-B PMs is one way for improving the magnetic properties of Ce-Fe-B magnet [103], [104]. By doing this, due to the formation of a layer with high anisotropy on the surface of $Ce_2Fe_{14}B$ grains, the anisotropy is considerably increased and $(BH)_{max}$ reaches to 10.8 MGOe (86 kJ/m^3) [103]. The corrosion tendency and the corrosion speed of Nd-Fe-B PM decrease by alloying [105].

Partial substitution of Ce for Nd in $Nd_2Fe_{14}B$ is another approach for improving the cerium PM properties [99], [100], [104]. The maximum amount of this substitution which does not dramatically attenuate the magnetic properties is 38%. In this manner, the 586 K Curie temperature of $Nd_2Fe_{14}B$ gets to 543 K for $(Nd_{0.62}Ce_{0.38})_2Fe_{14}B$ [100].

For cerium magnet, replacing a portion of iron with Co results into the increase of Curie temperature and $(BH)_{max}$. The maximum magnetic energy of $(Nd_{0.8}Ce_{0.2})_{2.4}Fe_{12}Co_2B$ produced by die upsetting technique has been reported to be 31.2 MGOe (248.35 kJ/m^3) at room temperature [99].

Simultaneous substitution of Ce and Y (yttrium) for Nd increases the thermal stability of the PM, yet the magnetic properties are not deteriorated. In case of replacing 9%wt Ce-Y (4.2%w Y), the $(BH)_{max}$ value decreases from 47.6 MGOe to 45.6 MGOe, but the temperature coefficient of H_c would be 0.9% lower comparing with Nd-Fe-B (its reduction with temperature is smaller) [102]. Table 8 presents different compositions of Ce-Nd-Fe-B PM and their magnetic properties.

4.8. Sm-Fe-N PM

The $Sm_2Fe_{17}N_3$ PM, which is obtained by nitrogenation of Sm_2Fe_{17}, could be considered as another substitute of RE PMs [38]. Although this less studied magnet shows a lower magnetization than the $Nd_2Fe_{14}B$ PM, but its magnetocrystalline anisotropy and Curie temperature are higher [106] (The Curie temperature of $Sm_2Fe_{17}N_3$ is 477 °C [107]). The powder of this magnet has been synthesized by low-temperature ball milling [107], high-energy ball milling [108], and reduction-diffusion [38], [109] techniques. The latter has resulted in a $(BH)_{max}$ of 40.58 MGOe (323 kJ/m^3), but forming the obtained powder as bulk pieces reduces the $(BH)_{max}$ (17.58 MGOe (140 kJ/m^3)) [38].

5. COMPARING SOME MAGNETIC PROPERTIES OF VARIOUS PMS

The highest reported values of $(BH)_{max}$ for different PMs are given in Fig. 23.

TABLE 8: MAGNETIC PROPERTIES OF VARIOUS CE-ND-FE-B PM COMPOUNDS [99], [101], [102], [103], [104].

Compound	$(BH)_{max}$	
	MGOe	kJ/m^3
$Ce_{12}Fe_{82}B_6$	5.57	44.33
$Ce_{13.5}Fe_{80.5}B_6$	6.8	54.12
$Nd_2Fe_{14}B/Ce_2Fe_{14}B$ alloy	10.8	86
$(Nd_{0.8}Ce_{0.2})_{2.4}Fe_{12}Co_2B$	31.2	248.35
9%wt Y-Ce Co-substituted Nd magnet	45.6	363

It is observed that except $Ce_{13.5}Fe_{80.5}B_6$, other new-generation magnets possess higher $(BH)_{max}$ compared to ferrite and alnico PMs. Furthermore, in comparison with $SmCo_5$, exchange spring (Nd-Fe-B, Fe-Co) PM, $Fe_{16}N_2$, $L1_0$ Fe-Ni, MnGa, cobalt nanorods, $(Nd_{0.8}Ce_{0.2})_{2.4}Fe_{12}Co_2B$ cerium PM, and $Sm_2Fe_{17}N_3$ show higher magnetic energy. The highest practically calculated magnetic energy belongs to the exchange spring PM (Nd-Fe-B, Fe-Co). However, theoretically, $Fe_{16}N_2$ exhibits a good potential for producing high-energy magnets.

6. CONCLUSIONS

Various compounds of PMs with diverse magnetizations and working temperatures have been investigated for several different applications heretofore. Among them, Alnico, ferrite, samarium-cobalt, and Nd-Fe-B PMs have been manufactured industrially and have been used in electric machines. Alnico and ferrite magnets, due to relatively poor magnetic properties compared to other types, are rarely utilized in applications, which require high magnetization or high magnetic energy. However, PMs containing rare earth elements, i.e. Sm-Co and Nd-Fe-B, thanks to their superb magnetic characteristics (e.g. high (BH)max), have been abundantly studied and employed. Currently, many studies on improving the properties of these magnets are carried out. Unfortunately, the resources of REEs are exclusive and there has been a global rise in their prices. Accordingly, researchers have sought some approaches for reducing the consumption of these elements or replacing RE PMs by other types of PMs, while preserving their magnetic properties. The studied magnet types for this purpose include exchange bias, exchange spring, nitrogen martensite (α'-$Fe_{16}N_2$), compounds with $L1_0$ structure, Fe-Ni, MnGa, and other compounds, which are addressed as new-generation PMs. The review of previous works revealed that among new- generation PMs, exchange spring, α'-$Fe_{16}N_2$, $L1_0$ Fe-Ni, and MnGa magnets possess proper theoretical and practical magnetic properties. They have a very good potential for replacing RE PMs, if their stable phase in bulk pieces could be produced by affordable techniques.

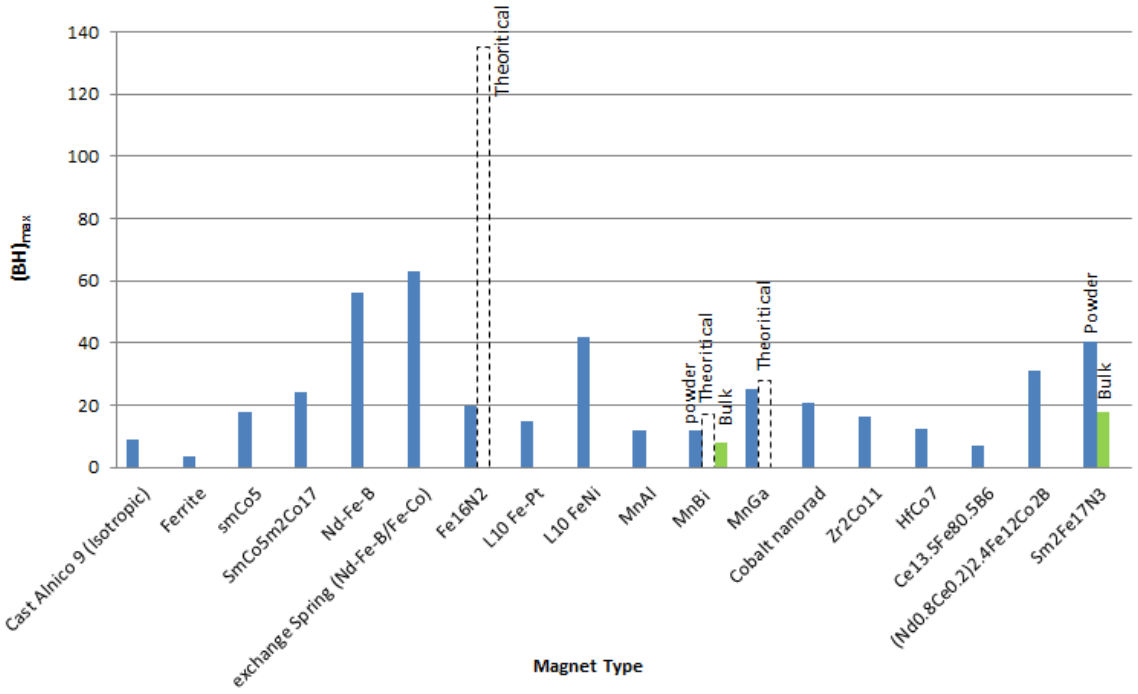

Fig. 23: The highest reported $(BH)_{max}$ for various PMs

REFERENCES

[1] O. Ben Dor, S. Yochelis, S. P. Mathew, R. Naaman, and Y. Paltiel, "A chiral-based magnetic memory device without a permanent magnet," Nat. Commun., vol. 4, p. 2256, 2013.

[2] C. T. Sherman, P. K. Wright, and R. M. White, "Physical Validation and testing of a MEMS piezoelectric permanent magnet current sensor with vibration canceling," Sensors Actuators A. Phys., vol. 248, pp. 206–213, 2016.

[3] J. M. D. Coey, "Permanent magnet applications," J. Magn. Magn. Mater., vol. 248, no. 3, pp. 441–456, 2002.

[4] J. V. M. Mcginley, M. Ristic, and I. R. Young, "A permanent MRI magnet for magic angle imaging having its field parallel to the poles," J. Magn. Reson., vol. 271, pp. 60–67, 2016.

[5] F. Jimenez-villacorta and L. H. Lewis, "Advanced Permanent Magnetic Materials," NANOMAGNETISM, pp. 160–189, 2014.

[6] F. JACEK and GIERAS, "Permanent Magnet Motor Technology: Design and Applications". CRC Press Taylor & Francis Group, 2010.

[7] M. Lak, "Speed Control for Direct Drive Permanent Magnet Wind Turbine," no. Figure 1, pp. 317–321, 2014.

[8] J. D. Widmer, R. Martin, and M. Kimiabeigi, "Sustainable Materials and Technologies Electric vehicle traction motors without rare earth magnets," SUSMAT, vol. 3, pp. 7–13, 2015.

[9] Z. Xu, A. Al-Timimy, and M. Degano, "Thermal management of a permanent magnet motor for an directly coupled pump," in Industrial Electronics Society IECON 2016 - 42nd Annual Conference of the IEEE, 2016, pp. 1749–1754.

[10] I. I. Abdalla, T. Ibrahim, and N. Bin Mohd Nor, "Development and optimization of a moving-magnet tubular linear permanent magnet motor for use in a reciprocating compressor of household refrigerators," Int. J. Electr. Power Energy Syst., vol. 77, pp. 263–270, 2016.

[11] L. I. X. Jime, "Perspectives on Permanent Magnetic Materials for Energy Conversion and Power Generation," Metall Mater Trans A 44 (Suppl 1), 2–20 (2013).

[12] "Rare-Earth Permanent Magnets, Vacodym and Vacomax," Vacuumschmelze GmbH Co. KG, http//www.vacuumschmelze.com/fileadmin/Medienbibliothek_2010/Downloads/DM/VACODYM-VACOMAX-PD002_2015_en.pdf.

[13] B. D. Cullity and C. D. Geraham, "introduction to Magnetic materilas," John Wiley & Sons, 2009.

[14] E. Furlani, "permanent magnets and electrochemical devices." Elsevier, 2001.

[15] A. Goldman, "MODERN FERRITE TECHNOLOGY. Springer", 2006.
[16] Steve Constantinides, "Market Outlook for Ferrite, Rare Earth and Other Permanent Magnets: 2015 to 2025," Magn. 2017, pp. 1–43, 2016.
[17] R. C. Pullar, "Hexagonal ferrites: A review of the synthesis, properties and applications of hexaferrite ceramics," Prog. Mater. Sci., vol. 57, no. 7, pp. 1191–1334, Sep. 2012.
[18] D. Chen, D. Zeng, and Z. Liu, "Synthesis, structure, morphology evolution and magnetic properties of single domain strontium hexaferrite particles," Mater. Res. Express, vol. 3, no. 4, p. 45002, Apr. 2016.
[19] A. J. Moulson and J. M. Herbert, "Electroceramics: materials, properties, applications". John Wiley & Sons Ltd, 2003.
[20] J.M.D. Coey, "Magnetism and magnetic materilas." Cambridge University Press, 2010.
[21] O. Gutfleisch, M. a Willard, E. Brück, C. H. Chen, S. G. Sankar, and J. P. Liu, "Magnetic materials and devices for the 21st century: stronger, lighter, and more energy efficient.," Adv. Mater., vol. 23, no. 7, pp. 821–42, Feb. 2011.
[22] US Geological Survey, "Mineral Commodity Summaries 2016 Mineral Commodity Summaries 2016," 2016.
[23] J.M.D. Coey, "Perspective and Prospects for Rare Earth Permanent Magnets," Engineering, https://doi.org/10.1016/j.eng.2018.11.034
[24] H. S. Yoon, C. J. Kim, K. W. Chung, S. D. Kim, J. Y. Lee, and J. R. Kumar, "Solvent extraction, separation and recovery of dysprosium (Dy) and neodymium (Nd) from aqueous solutions: Waste recycling strategies for permanent magnet processing," Hydrometallurgy, vol. 165, pp. 27–43, 2016.
[25] R. Schulze and M. Buchert, "Estimates of global REE recycling potentials from NdFeB magnet material," Resour. Conserv. Recycl., vol. 113, pp. 12–27, 2016.
[26] V. Prakash, Z. H. I. Sun, J. Sietsma, and Y. Yang, "Simultaneous Electrochemical Recovery of Rare Earth Elements and Iron from Magnet Scrap: A Theoretical Analysis". Elsevier Inc., 2015.
[27] "Critical materilas sterategy." U.S. department of energy, 2010.
[28] T. Ogawa, Y. Ogata, R. Gallage, N. Kobayashi, N. Hayashi, Y. Kusano, S. Yamamoto, K. Kohara, M. Doi, M. Takano, and M. Takahashi, "Challenge to the Synthesis of α‣ -Fe16N2 Compound Nanoparticle with High Saturation Magnetization for Rare Earth Free New Permanent Magnetic Material," vol. 73007.
[29] T. Shima, T. Moriguchi, S. Mitani, and K. Takanashi, "Low-temperature fabrication of L10 ordered FePt alloy by alternate monatomic layer deposition," Appl. Phys. Lett., vol. 80, no. 2, p. 288, 2002.
[30] P. Campbell, "permanent magnet materials and their application." Cambridge University Press, 1994.
[31] W. Gong, X. Zhao, W. Fan, J. Feng, A. Lin, J. He, W. Liu, and Z. Zhang, "Structure, Magnetic Properties, and Coercivity Mechanism of Rapidly Quenched MnxGa Ribbons," IEEE Trans. Magn., vol. 51, no. 11, pp. 1–4, 2015.
[32] D. Jiles, "introduction to magnetism and magnetic materilas." SPRINGER-SCENCE+BUSINESS MEDIA, 1991.
[33] N. A. Spaldin, "Magnetic materilas". Cambridge University Press, 2011.
[34] S. P. Gubin, "Magnetic Nanoparticles". WILEY-VCH Verlag GmbH & Co.KGaA, 2009.
[35] X. H. Tan, S. F. Chan, K. Han, and H. Xu, "Combined effects of magnetic interaction and domain wall pinning on the coercivity in a bulk $Nd_{60}Fe_{30}Al_{10}$ ferromagnet.," Sci. Rep., vol. 4, p. 6805, Jan. 2014.
[36] Zhongwu Liu a, Jiayi He , Qing Zhou, Youlin Huang, Qingzheng Jiang," Development of non-rare earth grain boundary modification techniques for Nd-Fe-B permanent magnets", Journal of Materials Science & Technology,vol. 98, pp.51–61, 2022.
[37] L. Zheng, B. Cui, L. Zhao, W. Li, and G. C. Hadjipanayis, "Sm2Co17 nanoparticles synthesized by surfactant-assisted high energy ball milling," J. Alloys Compd., vol. 539, pp. 69–73, Oct. 2012.
[38] S. Sugimoto, "Current status and recent topics of rare-earth permanent magnets," J. Phys. D. Appl. Phys., vol. 44, p. 64001, 2011.
[39] S. Pan, "Rare Earth Permanent-Magnet Alloys-High Temperature Phase Transformation: In Situ and Dynamic Observation and Its Application in Materials Design". Springer, 2013.
[40] J. S. M. J. Noguesa, J. Sort, V. Langlais, V. Skumryev, S. Surinach and Baro, "Exchange bias in nanostructures," Phys. Rep., vol. 22, pp. 65–117, 2005.
[41] J. S. Jiang and S. D. Bader, "Rational design of the exchange-spring permanent magnet," J. Phys. Condens. Matter, vol. 26, no. 6, p. 64214, Feb. 2014.
[42] A. López-Ortega, M. Estrader, G. Salazar-Alvarez, A. G. Roca, and J. Nogués, "Applications of exchange coupled bi-magnetic hard/soft and soft/hard magnetic core/shell nanoparticles" Phys. Rep., vol. 553, no. 2014, pp. 1–32, Feb. 2015.
[43] W.-B. Cui, Y. K. Takahashi, and K. Hono, "Nd2Fe14B/FeCo anisotropic nanocomposite films with a large maximum energy product" Adv. Mater., vol. 24, no. 48, pp. 6530–5, Dec. 2012.
[44] G. Giannopoulos, L. Reichel, A. Markou, I. Panagiotopoulos, and V. Psycharis, "Optimization of L1 0 FePt / Fe 45 Co 55 thin films for rare earth free permanent magnet applications," vol. 223909, pp. 1–8, 2015.
[45] V. Neu, S. Sawatzki, M. Kopte, C. Mickel, and L. Schultz, "Fully epitaxial, exchange coupled SmCo 5/Fe multilayers with energy densities above 400 kJ/m 3," IEEE Trans. Magn., vol. 48, no. 11, pp. 3599–3602, 2012.
[46] N. Route and N. Magnets, "A Novel Rout for the Preparation of Nanocomposit Magnets," pp. 1441–1444, 2000.
[47] S. Sun, "Exchange-coupled nanocomposite magnets by nanoparticle," no. November, pp. 395–398, 2002.
[48] R. Goyal, N. Arora, A. Kapoor, S. Lamba, and S. Annapoorni, "Exchange hardening in FePt/Fe3Pt dual exchange spring magnet: Monte Carlo modeling," J. Alloys Compd., vol. 695, pp. 1014–1019, 2017.

[49] J. Zhou, R. Skomski, X. Li, W. Tang, G. C. Hadjipanayis, and D. J. Sellmyer, "Permanent-Magnet Properties of Thermally Processed FePt and FePt – Fe Multilayer Films," no. SEPTEMBER, pp. 2802–2804, 2002.

[50] B. Balasubramanian, B. Das, R. Skomski, W. Y. Zhang, and D. J. Sellmyer, "Novel nanostructured rare-earth-free magnetic materials with high energy products" Adv. Mater., vol. 25, no. 42, pp. 6090–3, Nov. 2013.

[51] a. D. Volodchenkov, Y. Kodera, and J. E. Garay, "Synthesis of strontium ferrite/iron oxide exchange coupled nano-powders with improved energy product for rare earth free permanent magnet applications," J. Mater. Chem. C, 2016.

[52] R. W. McCallum, L. Lewis, R. Skomski, M. J. Kramer, and I. E. Anderson, "Practical Aspects of Modern and Future Permanent Magnets" Annu. Rev. Mater. Res., vol. 44, no. 1, pp. 451–477, Jul. 2014.

[53] A. Poorbafrani, H. Salamati, and P. Kameli, "Exchange spring behavior in Co0.6Zn0.4Fe2O4/SrFe10.5O16.75 nanocomposites," Ceram. Int., vol. 41, no. 1, pp. 1603–1608, 2015.

[54] R. Safi, A. Ghasemi, and R. Shoja-Razavi, "The role of shell thickness on the exchange spring mechanism of cobalt ferrite/iron cobalt magnetic nanocomposites," Ceram. Int., vol. 43, no. 1, pp. 617–624, 2017.

[55] Y. Jiang, M. Al Mehedi, E. Fu, Y. Wang, L. F. Allard, and J.-P. Wang, "Synthesis of α‧-Fe16N2 compound Free-Standing Foils with 20 MGOe Magnetic Energy Product by Nitrogen Ion-Implantation," Nat. Sci. Reports, vol. 6, no. November 2015, p. 25436, 2016.

[56] Y. Jiang, V. Dabade, L. F. Allard, E. Lara-Curzio, R. James, and J. P. Wang, "Synthesis of α‧-Fe16N2 Compound Anisotropic Magnet by the Strained-Wire Method," Phys. Rev. Appl., vol. 6, no. 2, pp. 1–10, 2016.

[57] I. Dirba, C. A. Schwobel, L. V. B. Diop, M. Duerrschnabel, L. Molina-Luna, K. Hofmann, P. Komissinskiy, H. J. Kleebe, and O. Gutfleisch, "Synthesis, morphology, thermal stability and magnetic properties of α‧-Fe16N2 nanoparticles obtained by hydrogen reduction of γ-Fe2O3 and subsequent nitrogenation," Acta Mater., vol. 123, pp. 214–222, 2017.

[58] T. Ogi, Q. Li, S. Horie, A. Tameka, T. Iwaki, and K. Okuyama, "α-hematite for rare-earth-free magnet applications Synthesis process," Adv. Powder Technol., 2016.

[59] Y. Jiang, B. Himmetoglu, M. Cococcioni, and J.-P. Wang, "DFT calculation and experimental investigation of Mn doping effect in Fe16N2," AIP Adv., no. 5, p. 56007, 2016.

[60] J.-P. Wang, S. He, and Y. Jiang, "Iron nitride permanent magnet and technique for forming iron nitride permanent magnet," 2014.

[61] H. Zeng, M. L. Yan, N. Powers, and D. J. Sellmyer, "Orientation-controlled nonepitaxial $L1_0$ CoPt and FePt films," Appl. Phys. Lett., vol. 80, no. 13, p. 2350, 2002.

[62] A. M. Montes-Arango, L. G. Marshall, A. D. Fortes, N. C. Bordeaux, S. Langridge, K. Barmak, and L. H. Lewis, "Discovery of process-induced tetragonality in equiatomic ferromagnetic FeNi," Acta Mater., vol. 116, pp. 263–269, 2016.

[63] T. Kojima, M. Ogiwara, M. Mizuguchi, M. Kotsugi, T. Koganezawa, T. Ohtsuki, T.-Y. Tashiro, and K. Takanashi, "Fe-Ni composition dependence of magnetic anisotropy in artificially fabricated L10-ordered FeNi films.," J. Phys. Condens. Matter, vol. 26, no. 6, p. 64207, Feb. 2014.

[64] L. H. Lewis, a Mubarok, E. Poirier, N. Bordeaux, P. Manchanda, a Kashyap, R. Skomski, J. Goldstein, F. E. Pinkerton, R. K. Mishra, R. C. Kubic, and K. Barmak, "Inspired by nature: investigating tetrataenite for permanent magnet applications.," J. Phys. Condens. Matter, vol. 26, no. 6, p. 64213, Feb. 2014.

[65] E. Poirier, F. E. Pinkerton, R. Kubic, R. K. Mishra, N. Bordeaux, A. Mubarok, L. H. Lewis, J. I. Goldstein, R. Skomski, and K. Barmak, "Intrinsic magnetic properties of L10 FeNi obtained from meteorite NWA 6259," J. Appl. Phys., vol. 117, no. 17, p. 17E318, May 2015.

[66] M. Kotsugi, H. Maruyama, N. Ishimatsu, N. Kawamura, M. Suzuki, M. Mizumaki, K. Osaka, T. Matsumoto, T. Ohkochi, and T. Ohtsuki, "Structural, magnetic and electronic state characterization of L10-type ordered FeNi alloy extracted from a natural meteorite.," J. Phys. Condens. Matter, vol. 26, no. 6, p. 64206, Feb. 2014.

[67] J. Liu and K. Barmak, "Interdiffusion in nanometric Fe/Ni multilayer films," J. Vac. Sci. & Technol. A Vacuum, Surfaces, Film., vol. 33, no. 2, p. 21510, 2015.

[68] L. Néel, J. Pauleve, R. Pauthenet, J. Laugier, and D. Dautreppe, "Magnetic Properties of an Iron—Nickel Single Crystal Ordered by Neutron Bombardment," J. Appl. Phys., vol. 35, no. 3, p. 873, 1964.

[69] T. Shima, M. Okamura, S. Mitani, and K. Takanashi, "Structure and magnetic properties for L10-ordered FeNi films prepared by alternate monatomic layer deposition," J. Magn. Magn. Mater., vol. 310, no. 2, pp. 2213–2214, Mar. 2007.

[70] T. Kojima, M. Mizuguchi, and K. Takanashi, "Growth of L10-FeNi thin films on Cu(001) single crystal substrates using oxygen and gold surfactants," Thin Solid Films, vol. 603, pp. 348–352, 2016.

[71] J. M. D. Coey, "New permanent magnets; manganese compounds," J. Phys. Condens. Matter, vol. 26, no. 6, p. 64211, Feb. 2014.

[72] R. Ducher, R. Kainuma, and K. Ishida, "Phase equilibria in the Ni-rich portion of the Ni-Ga binary system," Intermetallics, vol. 15, no. 2, pp. 148–153, 2007.

[73] Q. Zeng, I. Baker, and Z. C. Yan, "Nanostructured Mn-Al permanent magnets produced by mechanical milling," J. Appl. Phys., vol. 99, no. 8, pp. 16–19, 2006.

[74] A. Chaturvedi, R. Yaqub, and I. Baker, "A comparison of τ-MnAl particulates produced via different routes," J. Phys. Condens. Matter, vol. 26, no. 6, p. 64201, Feb. 2014.

[75] a Pasko, M. LoBue, E. Fazakas, L. K. Varga, and F. Mazaleyrat, "Spark plasma sintering of Mn-Al-C hard magnets.," J. Phys. Condens. Matter, vol. 26, no. 6, p. 64203, Feb. 2014.

[76] N. Singh, R. Shyam, N. K. Upadhyay, and a Dhar, "Development of Rare-Earth Free Mn-Al Permanent Magnet Employing Powder Metallurgy Route," IOP Conf. Ser. Mater. Sci. Eng., vol. 73, p. 12042, Feb. 2015.

[77] M. Gjoka, C. Sarafidis, G. Giannopoulos, and D. Niarchos, "Effects of milling conditions on the magnetic properties of MnBi alloys," 2015 IEEE Int. Magn. Conf. INTERMAG 2015.

[78] J. Park, Y.-K. Hong, J. Lee, W. Lee, S.-G. Kim, and C.-J. Choi, "Electronic Structure and Maximum Energy Product of MnBi," Metals (Basel), vol. 4, no. 3, pp. 455–464, Aug. 2014.

[79] Ronald, Pirich, David, and Larson, "Directional solidification and densification of permanent magnets having single domain size MnBi particles," 1988.

[80] J. B. Yang, Y. B. Yang, X. G. Chen, X. B. Ma, J. Z. Han, Y. C. Yang, S. Guo, a. R. Yan, Q. Z. Huang, M. M. Wu, and D. F. Chen, "Anisotropic nanocrystalline MnBi with high coercivity at high temperature," Appl. Phys. Lett., vol. 99, no. 8, p. 82505, 2011.

[81] H. Kronmüller, J. B. Yang, and D. Goll, "Micromagnetic analysis of the hardening mechanisms of nanocrystalline MnBi and nanopatterned FePt intermetallic compounds," J. Phys. Condens. Matter, vol. 26, no. 6, p. 64210, Feb. 2014.

[82] N. V Rama Rao, a. M. Gabay, and G. C. Hadjipanayis, "Anisotropic fully dense MnBi permanent magnet with high energy product and high coercivity at elevated temperatures," J. Phys. D. Appl. Phys., vol. 46, no. 6, p. 62001, 2013.

[83] J. Cui, J. P. Choi, G. Li, E. Polikarpov, J. Darsell, N. Overman, M. Olszta, D. Schreiber, M. Bowden, and T. Droubay, "Thermal stability of MnBi magnetic materials.," J. Phys. Condens. Matter, vol. 26, no. 6, p. 64212, Feb. 2014.

[84] D. T. Zhang, S. Cao, M. Yue, W. Q. Liu, J. X. Zhang, and Y. Qiang, "Structural and magnetic properties of bulk MnBi permanent magnets," J. Appl. Phys., vol. 109, no. 7, p. 07A722, 2011.

[85] V. Ly, X. Wu, L. Smillie, T. Shoji, A. Kato, A. Manabe, and K. Suzuki, "Low-temperature phase MnBi compound: A potential candidate for rare-earth free permanent magnets," J. Alloys Compd., vol. 615, no. S1, pp. S285–S290, 2015.

[86] L. Zhu, S. Nie, K. Meng, D. Pan, J. Zhao, and H. Zheng, "Multifunctional $L1_0$-$Mn_{1.5}Ga$ films with ultrahigh coercivity, giant perpendicular magnetocrystalline anisotropy and large magnetic energy product.," Adv. Mater., vol. 24, no. 33, pp. 4547–51, Aug. 2012.

[87] R. Rejali, D. H. Ryan, Z. Altounian, C. B. Boyer, Q. Lu, M. Wang, H. Zhang, and M. Yue, "Crystal structure and magnetism of the MnxGa ($1.15 \leq x \leq 2.0$) rare-earth-free permanent magnet system," AIP Adv., vol. 6, no. 5, pp. 1–8, 2016.

[88] B. Z. Cui, M. Marinescu, and J. F. Liu, "Ferromagnetic tetragonal L10-Type MnGa isotropic nanocrystalline microparticles," IEEE Trans. Magn., vol. 49, no. 7, pp. 3322–3325, 2013.

[89] Q. Lu, M. Wang, H. Zhang, and M. Yue, "Microstructure and Improved Coercivity of Mn 1.33 Ga Nanoflakes by Surfactant-Assisted Ball Milling", IEEE International Magnetic Conference, 2015.

[90] H. Zhao, W. Y. Yang, Z. Y. Shao, G. Tian, D. Zhou, X. P. Chen, Y. H. Xia, L. Xie, S. Q. Liu, H. L. Du, J. Z. Han, C. S. Wang, Y. C. Yang, and J. B. Yang, "Structural evolution and magnetic properties of L10-type $Mn_{54.5}Al_{45.5-x}Ga_x$ (x = 0.0, 15.0, 25.0, 35.0, 45.5) phase," J. Alloys Compd., vol. 680, pp. 14–19, 2016.

[91] J. N. Feng, W. Liu, W. J. Gong, X. G. Zhao, D. Kim, C. J. Choi, and Z. D. Zhang, "Magnetic Properties and Coercivity of MnGa Films Deposited on Different Substrates," J. Mater. Sci. Technol., 2016.

[92] J. FENG "Magnetic properties and coercivity mechanism of MnGa films" pp. 2015, 2015.

[93] I. P. and G. V. E. Anagnostopoulou, B. Grindi, L.-M. Lacroix, F. Ott, "Dense arrays of cobalt nanorods as rare-earth free permanent magnets," Nanoscale, vol. 8, no. 7, pp. 4020–4029, 2016.

[94] M. Sarr, N. Bahlawane, D. Arl, M. Dossot, E. McRae, and D. Lenoble, "Atomic layer deposition of cobalt carbide films and their magnetic properties using propanol as a reducing agent," Appl. Surf. Sci., vol. 379, pp. 523–529, 2016.

[95] V. G. Harris, Y. Chen, A. Yang, S. Yoon, Z. Chen, A. L. Geiler, J. Gao, C. N. Chinnasamy, L. H. Lewis, C. Vittoria, E. E. Carpenter, K. J. Carroll, R. Goswami, M. A. Willard, L. Kurihara, M. Gjoka, and O. Kalogirou, "High coercivity cobalt carbide nanoparticles processed via polyol reaction: a new permanent magnet material," J. Phys. D. Appl. Phys., vol. 43, p. 165003, 2010.

[96] V. Harris and Sharon, "Cobalt Carbide-Based nanoparticle Permanent Magnet Materials," patent No. EP2475483A1, 2015.

[97] O. H. Materials, "Novel Functional Magnetic Materials". 1999.

[98] B. Balamurugan, B. Das, W. Y. Zhang, R. Skomski, and D. J. Sellmyer, "Hf-Co and Zr-Co alloys for rare-earth-free permanent magnets.," J. Phys. Condens. Matter, vol. 26, no. 6, p. 64204, Feb. 2014.

[99] A. K. Pathak, M. Khan, K. A. Gschneidner, R. W. McCallum, L. Zhou, K. Sun, K. W. Dennis, C. Zhou, F. E. Pinkerton, M. J. Kramer, and V. K. Pecharsky, "Cerium: An unlikely replacement of dysprosium in high performance Nd-Fe-B permanent magnets," Adv. Mater., vol. 27, no. 16, pp. 2663–2667, 2015.

[100] M. A. Susner, B. S. Conner, B. I. Saparov, M. A. McGuire, E. J. Crumlin, G. M. Veith, H. Cao, K. V. Shanavas, D. S. Parker, B. C. Chakoumakos, and B. C. Sales, "Flux growth and characterization of Ce-substituted Nd2Fe14B Single Crystal," J. Magn. Magn. Mater., 2016.

[101] Z. B. Li, M. Zhang, B. G. Shen, F. X. Hu, and J. R. Sun, "Variations of phase constitution and magnetic properties with Ce content in Ce-Fe-B permanent magnets," Mater. Lett., vol. 172, pp. 102–104, 2016.

[102] Z. B. Li, B. G. Shen, M. Zhang, F. X. Hu, and J. R. Sun, "Substitution of Ce for Nd in preparing R2Fe14B nanocrystalline magnets," J. Alloys Compd., vol. 628, pp. 325–328, 2015.
[103] K. CHEN, S. GUO, X. FAN, G. DING, L. CHEN, R. CHEN, D. LEE, and A. YAN, "Coercivity enhancement of Ce-Fe-B sintered magnets by low-melting point intergranular additive," J. Rare Earths, vol. 35, no. 2, pp. 158–163, 2017.
[104] B. Peng, T. Ma, Y. Zhang, J. Jin, and M. Yan, "Improved thermal stability of Nd-Ce-Fe-B sintered magnets by Y substitution," Scr. Mater., vol. 131, pp. 11–14, 2017.
[105] E. Isotahdon, E. Huttunen-Saarivirta, and V.-T. Kuokkala, "Characterization of the microstructure and corrosion performance of Ce-alloyed Nd-Fe-B magnets," J. Alloys Compd., vol. 692, pp. 190–197, 2017.
[106] T. Saito and K. Kikuchi, "Production of Sm-Fe-N bulk magnets by the spark plasma sintering method with dynamic compression," J. Alloys Compd., 2016.
[107] Q. Fang, X. An, F. Wang, Y. Li, J. Du, W. Xia, A. Yan, J. P. Liu, and J. Zhang, "Journal of Magnetism and Magnetic Materials The structure and magnetic properties of Sm – Fe – N powders prepared by ball milling at low temperature," J. Magn. Mater., vol. 410, pp. 116–122, 2016.
[108] M. Yue, Y. Q. Li, R. M. Liu, W. Q. Liu, Z. H. Guo, and W. Li, "Abnormal size-dependent coercivity in ternary Sm – Fe – N nanoparticles," vol. 637, pp. 297–300, 2015.
[109] Y. Hirayama, A. K. Panda, T. Ohkubo, and K. Hono, "Scripta Materialia High coercivity Sm 2 Fe 17 N 3 submicron size powder prepared by polymerized-complex and reduction – diffusion process," SMM, vol. 120, pp. 27–30, 2016.